Biogeosciences Discuss., 12, 18723–18768, 2015
www.biogeosciences-discuss.net/12/18723/2015/
doi:10.5194/bgd-12-18723-2015

Biogeosciences Discussions
Open Access
EGU

Methods comparison to retrieve the refractive index of small scatterers

A.-M. Sánchez and J. Piera

Institute of Marine Sciences (ICM-CSIC), Physical and Technological Oceanography Department, Pg. Marítim de la Barceloneta, 37–49, 08003, Barcelona, Spain

Received: 9 October 2015 – Accepted: 30 October 2015 – Published: 24 November 2015

Correspondence to: A.-M. Sánchez (amsanchez@icm.csic.es)

Published by Copernicus Publications on behalf of the European Geosciences Union.

Abstract

Simulation tools to generate the inherent optical properties of small scatterers are useful to complement data difficult to measure, as for instance their angular scattering features. However, in most cases, shapes are reduced to homogeneous spheres, which is a gross simplification for any particles in water, and the inner complex refractive index is estimated using some approximations. In this paper, several methods for the retrieval of the refractive indices are used in three different examples modelling different shapes and particle size distributions. The error associated with each method is discussed and analysed. It is finally demonstrated that those inverse methods using a genetic algorithm provide optimal estimations relative to other techniques that, although faster, are less accurate. The obtained results suggest that phytoplankton models can be improved using this kind of algorithms and a suitable shape.

1 Introduction

The discrimination of water composition in marine environments is essential to understand the complex aquatic ecosystems, to early detect or predict harmful algal blooms (HABs), or to preserve and sustainably manage the marine resources. Water contents may include organic matter, such as phytoplankton, and inorganic matter, such as minerals or microplastics (Andrady, 2011; Cole et al., 2011). Since the component distribution strongly influences the propagation of light, the water content may be estimated from remote along with in situ light-propagation measurements if the inherent optical properties (IOPs) of each particle are well known, i.e., their absorption and scattering properties. However, actual instrumentation cannot provide an accurate characterization of a complete IOP (all angular scattering values are methodologically difficult to obtain), and therefore, particle modelling techniques become fundamental to complement the measured data.

BGD
12, 18723–18768, 2015

Lorenz–Mie and **T** Matrix theories have already been adopted to model living cells in water (such as phytoplankton cells, e.g. Quirantes and Bernard, 2006; Stramski et al., 2001) and suspended mineral particles (Twardowski et al., 2001). The first method is computationally faster than the latter but obtains the scattering angular distribution only from spheric shapes. However, only a minor number of phytoplankton species present a spheric shape. As shown by Clavano et al. (2007), aspect ratios of phytoplankton (ratio of the principal axes of a particle) span between 0.4 and 72. The second method, though slower, can be applied to model more complex shapes such as spheroids, cylinders or Chebyshev particles, and allows characterizing water components more accurately. In both cases, the particle inner complex refractive index must be known and, since ocean transmissometer measurements do not directly provide it, it must be estimated somehow (Aas, 1996).

Several inverse models to retrieve the refractive index from optical measurements can be found in the literature. For instance, a single equation based on the Lorenz–Mie theory is used by Twardowski et al. (2001), to estimate the bulk refractive index of water particles. It is indeed a fast method if optical backscattering measurements are feasible. Stramski et al. (1988) presented an extension of a model from Bricaud and Morel (1986), based on the anomalous diffraction approximation (ADA), which allows the computation of the real and imaginary parts of the complex refractive index as separate variables using only the absorption and attenuation efficiency factors and the particle size distribution (PSD). And Bernard et al. (2001) simplified this model by replacing the Lorentzian oscillators with a simple Hilbert transform. All these methods share one thing in common, they approximate the shape of the particles to homogeneous spheres. Meyer (1979) first and Bernard et al. (2009) later suggested that two-layered spherical geometry models reproduce more accurately the measured algal angular scattering properties. Finally, a combination of a genetic algorithm with the Lorenz–Mie and **T** Matrix approaches was used by Sánchez et al. (2014), thereby allowing more complex structures than simple homogeneous or coated spheres. A genetic algorithm is a search heuristic for optimization problems that simulates the pro-

BGD
12, 18723–18768, 2015

cess of natural selection using inheritance, mutation, selection, and crossover between different possible solutions. Again, this method only requires the measured attenuation and scattering coefficients, and the PSD to find the complex refractive index. Although it is a slow method (in particular, for non-spherical particles), it can provide very accurate estimations.

In this paper, the refractive index retrieval models mentioned above are reviewed and tested with three simulated examples in order to analyse their accuracy when modelling real particles suspended in water such as phytoplankton. To this end, the simulated examples are implemented using complex refractive indices and PSDs similar to those found in nature for phytoplankton species. Since phytoplankton particles exhibit a wide variety of shapes, each example has been provided with a different outline, accounting for a homogeneous sphere, a coated sphere and a homogeneous cylinder. None of these idealized models is an exact representation of a real algae presenting cell walls, chloroplasts, vacuole, nucleus and other internal organelles, each with its own optical properties. However, they can be considered a first approximation suitable for the purposes of this paper.

In order to establish the foundations of the work presented in this paper, Sect. 2 reviews the formulation to obtain the IOPs from Lorenz–Mie and **T** Matrix characterizations (that perform the forward calculations) for polydispersed algal assemblages. In Sect. 3, a review of the different inverse approximations to retrieve the refractive index is described. In Sect. 4, all the models are used to retrieve the refractive index of three synthetic particles. Section 5 discusses the results and finally, the conclusions are outlined in Sect. 6.

BGD
12, 18723–18768, 2015

2 Model theory

2.1 Inherent optical properties

Lorenz–Mie and **T** Matrix theories are powerful methods to formulate an analytical solution to electromagnetic scattering by spherical and non-spherical particles. Both rely on the expansion of the incoming light into spherical harmonics and use an intensive formulation to compute the coefficients that link the incident field with the scattered and transmitted ones. The complete Lorenz–Mie derivation is reviewed by Bohren and Huffman (1998), and the **T** Matrix approach is described by Mischenko et al. (1996). Both theories provide the particle specific optical properties, i.e., the extinction, scattering and absorption cross sections (which describe the area of the incident-beam intensity converted to extincted, scattered or absorbed light), C_{EXT}, C_{SCA} and C_{ABS} respectively. Using the obtained cross sections (size-averaged in polydisperse concentrations), the wavelength-dependent extinction, scattering and absorption coefficients ($c(\lambda)$, $b(\lambda)$ and $a(\lambda)$ respectively) can be computed as:

$$c(\lambda) = N \cdot \langle C_{\mathrm{EXT}}(\lambda) \rangle, \quad (1)$$

$$b(\lambda) = N \cdot \langle C_{\mathrm{SCA}}(\lambda) \rangle, \quad (2)$$

$$a(\lambda) = N \cdot \langle C_{\mathrm{ABS}}(\lambda) \rangle, \quad (3)$$

where N denotes the number of particles per unit volume and λ the wavelength. The relationship between the three parameters is:

$$c(\lambda) = a(\lambda) + b(\lambda). \quad (4)$$

Scattering can be further characterized in terms of the angular distribution of the scattered light using the volume scattering function (β) as:

$$\beta(\Psi, \lambda) = \widetilde{\beta}(\Psi, \lambda) \cdot b(\lambda). \quad (5)$$

BGD
12, 18723–18768, 2015

Ψ is the scattering angle (i.e., the angle between the incident and scattered beams) and $\widetilde{\beta}(\Psi,\lambda)$ is the volume scattering phase function and the first parameter of the Stokes scattering matrix. This matrix transforms the Stokes parameters of the incident light into those of the scattered light and it is obtained with the Lorenz–Mie and **T** Matrix formulation when the physical characteristics of the particles are known. The integral scattering in all directions, assuming azimuthal symmetry to preferential orientation, retrieves the total scattering coefficient b:

$$b(\lambda) = 2\pi \int_0^{\pi} \beta(\Psi,\lambda)\sin(\Psi)\mathrm{d}\Psi, \tag{6}$$

which can be partitioned into its forward and backward components (b_f and b_b respectively) by limiting the integration bounds from 0 to $\pi/2$ and from $\pi/2$ to π respectively. The backscatter fraction, defined by:

$$B_\mathrm{b}(\lambda) = \frac{b_\mathrm{b}(\lambda)}{b(\lambda)}. \tag{7}$$

gives the fraction of scattered light that is deflected through the scattering angles beyond $\pi/2$. Given Eqs. (5) and (6), the normalization condition for the volume scattering phase function is:

$$2\pi \int_0^{\pi} \widetilde{\beta}(\Psi,\lambda)\sin(\Psi)\mathrm{d}\Psi = 1. \tag{8}$$

This normalization implies that the backscatter fraction can be computed using the volume scattering phase function as:

$$B_\mathrm{b}(\Psi,\lambda) = 2\pi \int_{\frac{\pi}{2}}^{\pi} \widetilde{\beta}(\Psi,\lambda)\sin(\Psi)\mathrm{d}\Psi. \tag{9}$$

BGD
12, 18723–18768, 2015

The normalization factor 2π used in Eqs. (6), (8) and (9) is different from that used by Mischenko et al. (1996); Mischenko and Travis (1998); Wiscombe and Grams (1976); Mugnai and Wiscombe (1986), but used by Twardowski et al. (2001); Bohren and Huffman (1998), and most of the books in Ocean Optics, and therefore, applied here.

2.2 Size distributions and polydispersions

Algal assemblages are typically polydispersed with regard to size, and can be described by a PSD $F(d)$, where d is the particle diameter, and $F(d)\mathrm{d}(d)$ is the number of particles per unit volume in the size range $d \pm 1/2\mathrm{d}(d)$. Using absorption as an example (analogous expressions may be used for the other coefficients), the absorption efficiency factor representing the mean of a size distribution can be described as (Bricaud and Morel, 1986):

$$\overline{Q}_\mathrm{a} = \frac{\int_0^\infty Q_\mathrm{a}\, F(d) d^2 \mathrm{d}(d)}{\int_0^\infty F(d) d^2 \mathrm{d}(d)}. \tag{10}$$

The relationship between the absorption efficiency factor and the absorption cross section is:

$$Q_\mathrm{a} = \frac{C_\mathrm{a}}{G}, \tag{11}$$

being G the geometric cross section of the particle. And the resultant volume absorption coefficient is given by either:

$$a = \frac{\pi}{4} \int_0^\infty Q_\mathrm{a}\, F(d) d^2 \mathrm{d}(d), \tag{12}$$

BGD
12, 18723–18768, 2015

or, if the result of Eq. (10) is used:

$$a = \frac{\pi}{4}\overline{Q}_a \int_0^\infty F(d)d^2\mathrm{d}(d). \tag{13}$$

3 Review of refractive index retrieval models

In this section, a review of the different approximations to retrieve the refractive index is presented. Each method is named using the surname of one of the authors who published it. The complex refractive index $m(\lambda)$ is defined as:

$$m(\lambda) = n(\lambda) + ik(\lambda), \tag{14}$$

where the real part $n(\lambda)$ determines the phase velocity of the propagating wave, and the imaginary part $k(\lambda)$ determines the flux decay. Note that the effective refractive index is a relative value dependent upon the surrounding medium. This paper assumes as the relative refractive index in water $m_{\mathrm{water}} = 1.334 + i0$ (Hale and Querry, 1973).

3.1 The Twardowski model

The Twardowski model, presented by (Twardowski et al., 2001), is based on Volz (1954) as cited in van de Hulst (1957). It is derived using the Lorenz–Mie theory and the relationship between the particulate spectral attenuation ($c_p(\lambda)$) and the size distribution to retrieve the bulk particulate refractive index from in situ optical measurements. In particular, assumes that $\gamma = \xi - 3$, being γ the hyperbolic slope of the attenuation coefficient and ξ the power-law slope of the PSD. It only considers power-law distributions that fulfil the conditions $2.5 \leq \xi \leq 4.5$ and $0 \leq B_b \leq 0.03$. The bulk refractive index is obtained using a polynomial fit to the output of Lorenz–Mie calculations as:

$$\hat{m}(B_b, \gamma) = 1 + B_b^{0.5377+0.4867\gamma^2}\left(1.4676 + 2.2950\gamma^2 + 2.3113\gamma^4\right). \tag{15}$$

BGD
12, 18723–18768, 2015

This formulation is only exact for particles spanning from 0 to infinity which do not absorb (k is neglected) and are homogeneous spheres. It was first tested by Boss et al. (2001a) and refined in Boss et al. (2001b). It must be noted that the model is consistent with the measurements obtained from an AC9 with the scattering coefficient b serving as integrated scattering from 0.93 to 180°, which must be considered in Eq. (9). Even though this was not firstly considered in the calculations in Twardowski et al. (2001), it was taken into account in Boss et al. (2004), but the regression was not recomputed.

3.2 The Stramski model

This model is based on the methods presented by Stramski et al. (1988), which is an extension of that developed by Bricaud and Morel (1986). It is based on the ADA, first described in van de Hulst (1957). The ADA offers approximations to the absorption and attenuation optical efficiency factors using relatively simple algebraic formulae, based on the assumptions that the particle is large relative to wavelength ($\alpha = \frac{\pi d}{\lambda} \gg 1$) and the refractive index is small ($m - 1 \ll 1$ and $k \ll 1$). This method allows the effects of the real and imaginary refractive indices on absorption and scattering to be decoupled. Assuming homogeneous geometry, the ADA expression for the absorption efficiency factor is given by:

$$Q_a = 1 + \frac{2e^{-\rho'}}{\rho'} + 2\frac{e^{-\rho'} - 1}{\rho'^2}, \tag{16}$$

where $\rho' = 4\alpha k$ is the absorption optical thickness. Equations (13) and (16) are then used iteratively to determine the homogeneous imaginary part of the refractive index ($k(\lambda)$) in conjunction with measured algal absorption and PSD data. According to the Ketteler–Helmholtz theory of anomalous dispersion (van de Hulst, 1957), a variation in k induce variations in n, quantified with a series of oscillators (representing discrete absorption bands) based on the Lorentz–Lorentz equations (Stramski et al., 1988; Bricaud and Morel, 1986). These spectral variations (denoted as $\Delta n(\lambda)$) vary around

BGD
12, 18723–18768, 2015

a central part of the real refractive index $1+\epsilon$. Thus:

$$n(\lambda) = 1 + \epsilon + \Delta n(\lambda). \tag{17}$$

The central value $1+\epsilon$ is estimated by computing the nonabsorbing equivalent population attenuation efficiency factor $\left(\overline{\overline{Q}}_c^{\mathrm{NAE}}\right)$ at those wavelengths where $\Delta n(\lambda_\epsilon) = 0$. Considering polydispersion, this is done according to:

$$\overline{\overline{Q}}_c^{\mathrm{NAE}}(\overline{\rho}) = \frac{\int_0^\infty Q_c(\rho)F(\rho)\rho^2 \mathrm{d}(\rho)}{\int_0^\infty F(\rho)\rho^2 \mathrm{d}(\rho)}, \tag{18}$$

where $\rho = 2\alpha(n-1)$, $F(\rho)$ is obtained from the experimental size distribution by the replacement of d by ρ and $Q_c(\rho)$ from the van de Hulst's formula assuming $\xi = 0$ (van de Hulst, 1957):

$$Q_c = 2 - \frac{4}{\rho} sin\rho + \frac{4}{\rho^2}(1 - cos\rho). \tag{19}$$

The exact value of ϵ is indicated by such $\overline{\overline{Q}}_c^{\mathrm{NAE}}(\overline{\rho})$ that it equals $\overline{Q}_c(\lambda_\epsilon)$.

This methodology was latterly simplified by Bernard et al. (2001, 2009) by using the Kramers–Kronig relations to compute the spectral variations in the real part of the refractive index instead the Lorentzian oscillators. The Kramers–Kronig relations describe the mutual dependence of the real and imaginary parts of the refractive index through dispersion, as does Ketteler–Helmholtz theory, but they are more simply applied than the tedious and sometimes inaccurate use of summed oscillators (the real part is the Hilbert transform of the imaginary part, van de Hulst, 1957).

3.3 The Bernard model

Meyer (1979) and Bernard et al. (2009) suggested that two-layered spherical geometry models reproduce more accurately the measured algal angular scattering properties. In

BGD
12, 18723–18768, 2015

Bernard et al. (2009), the outer layer accounts for the chloroplast and the inner layer for the cytoplasm. Refractive index values are assumed for the cytoplasm, with a spectral imaginary part modelled as:

$$k_{\text{cyto}}(\lambda) = k_{\text{cyto}}(400)e^{[-0.01(\lambda-400)]}, \quad (20)$$

where $k_{\text{cyto}}(400) = 0.0005$. The real refractive index spectra for the cytoplasm, $n_{\text{cyto}}(\lambda)$, is obtained using the Hilbert transform (absorption has an influence on scattering and attenuation, expressed through the Kramers–Kronig relations) and Eq. (17) with $1+\epsilon = 1.02$. Using the $k_{\text{cyto}}(\lambda)$ of Eq. (20), volume equivalent $k_{\text{chlor}}(\lambda)$ are determined using the Gladstone–Dale formulation given by:

$$k_{\text{chlor}}(\lambda) = \frac{k_{\text{h}}(\lambda) - k_{\text{cyto}}(\lambda)\text{Vv}}{1 - \text{Vv}}, \quad (21)$$

where $k_{\text{h}}(\lambda)$ is the imaginary part of the refractive index considering homogeneous cells and obtained using Eq. (16), and Vv is the relative chloroplast volume. According to Bernard et al. (2009), a Vv value of 20 % can be considered as a first approximation for a spherical algal geometry, although higher values should be considered for the large celled dinoflagellate and crytophyte samples. Other previous studies have employed relative chloroplast volumes of Vv = 41 % (Zaneveld and Kitchen, 1995), Vv = 58 % (Latimer, 1984), and Vv = 27 to 66 % (Bricaud et al., 1992). The real refractive index spectra for the chloroplast $n_{\text{chlor}}(\lambda)$ is then similarly generated with a Hilbert transform and Eq. (17) with assumed $1+\epsilon$ values between 1.044 and 1.14 depending upon the sample.

3.4 The genetic algorithm model

The model presented by Sánchez et al. (2014) uses a genetic algorithm to find the refractive index that produces the desired scattering and absorption coefficients (*a* and *b*) when using the Lorenz–Mie or **T** Matrix approaches with the measured PSD.

BGD
12, 18723–18768, 2015

The performance of the algorithm can be summarized as follows (see Fig. 1). First, a random vector of solutions is generated for a specific wavelength ($[n_1(\lambda_i), n_2(\lambda_i), \ldots, n_n(\lambda_i)]$, where λ_i denotes the selected wavelength and $n_1, n_2, \ldots, n_n$ the complex refractive indices). If possible, the search space can be bounded in order to maximize the algorithm success. Then, the complete vector is evaluated by the fitness function. This is done by computing the a and b coefficients associated to each refractive index (using the Lorenz–Mie or **T** Matrix formulation and Eqs. 2–3) and evaluating the weighted euclidean distance between the calculated and desired coefficients. This can be obtained, for instance, as:

$$e_{\mathrm{a}} = |20\log(a_k(\lambda_i)) - 20\log(a_{\mathrm{m}}(\lambda_i))|, \tag{22}$$

where a_k is the calculated attenuation coefficient of the n_k refractive index, a_{m} is the desired (or measured) attenuation coefficient, and e_{a} is the committed error for the absorption coefficient. Using logarithmic values allows a suitable weighting factor when dealing with small errors over small coefficients. The same equation accounts for the scattering coefficient. Both results are finally combined using the quadratic mean, obtaining a single evaluation value that the algorithm tries to minimize.

After the evaluation, the algorithm may stop if either a maximum number of generations (each generation is a new vector of solutions) or a satisfactory fitness level have been reached. If the convergence condition is not fulfilled, the best solutions are selected and separated. Part of this elite is then recombined (crossover) and randomly mutated to provide genetic diversity and broaden the search space (crossover and mutation introduce the diversity needed to ensure that the entire sample space is reachable and avoid becoming stuck at suboptimal solutions, Greenhalgh and Marshall, 2000). The new set of solutions is re-evaluated and inserted again into the solutions' vector, which completes the cycle. After convergence is achieved, the algorithm presents the best solution it has been able to find.

Since Lorenz–Mie and **T** Matrix algorithms can only be executed for single wavelengths, and the refractive index is also wavelength dependent (with different values at

BGD
12, 18723–18768, 2015

different wavelengths), the genetic algorithm performs the search procedure at a single wavelength each time. After each convergence, the process starts again with the next wavelength-dependent values, eventually obtaining the complete complex-refractive-index signature.

The main advantage of this model is that it can be easily adapted to different Lorenz–Mie or **T** Matrix codes, as for instance those developed for homogeneous spheres, coated spheres, cylinders, etc. Besides it can also be easily combined with other models to improve the results. On the other hand, it must be noted, that some inversions could be ill-posed. A constrained optimization problem is considered to be well-posed in the sense of Haddamard if (a) a solution exists, (b) the solution is unique and (c) the solution is well-behaved, i.e. varies continuously with the problem parameters. An ill-posed problem fails to satisfy one or more of the aforementioned criteria (Bhandarkar et al., 1994). In that case, techniques such as regularization methods can be applied to improve the results (Mera et al., 2004).

4 Experimental simulations

The models described in the previous section are used here to retrieve the refractive index of well-known particles in order to determine their accuracy in estimating their refractive index and reproducing their IOPs. To this end, Sect. 4.1 deals with a simple spherical and homogeneous particle and presents the results provided by the Twardowski, Stramski and Genetic Algorithm models. Such particles, however, are not a fair representation of phytoplankton particles. First, because eukaryotic phytoplankton cells are heterogeneous particles with membrane systems and intracellular organelles, and second, because most of the phytoplankton species are not spherical. As stated by Bernard et al. (2009), the spherical structure mainly fails in the description of the backward scattering and suggests a two-layered spherical geometry as the simplest possible heterogeneous structure capable of reproducing measured algal angular scattering properties. In consequence, Sect. 4.2 presents a coated sphere as the initial

BGD
12, 18723–18768, 2015

particle and presents the estimated refractive indices provided by the genetic algorithm model, the Bernard model and a combination of both. Finally, Sect. 4.3 uses a cylindrical shape particle with a homogeneous refractive index. This shape was selected to be far different from a sphere and similar to that of some species of phytoplankton (as for instance, the diatom *Thalassiosira pseudonana*). Although this synthetic model do not exactly reproduce the same optical behaviour as the actual phytoplankton particle (the micro details of the cells are neglected), it can serve as a first approximation. Refractive index estimations provided by the combination of the genetic algorithm with the Bernard model for coated spheres and the Genetic Algorithm are shown.

4.1 Spherical-shape homogeneous particles

A concentration of 100 spherical particles mm^{-3} presenting the PSD of Fig. 2a (based on a power-law distribution – or Junge-type – with 51 points, $R_{min} = 0.7\,\mu m$, $R_{max} = 12.1\,\mu m$, a slop parameter $\xi = 3$, effective radius $r_{eff} = 4\,\mu m$ and effective variance $v_{eff} = 0.6$), along with the initial complex refractive index of Fig. 2b, was simulated using the Lorenz–Mie characterization (Bohren and Huffman, 1998). In particular, the BHMIE code, original from Bohren and Huffman and modified by B.T. Draine, was used (additional features were added, such as polydispersion and the computation of the Stokes scattering matrix). The obtained $a(\lambda)$, $b(\lambda)$ and $c(\lambda)$ coefficients are shown in Fig. 3a. As can be observed, the concentration was selected in order to obtain coefficient values similar to those measured by (Twardowski et al., 2001) and (Stramski et al., 2001). Although the power-law distribution is not a realistic distribution for single phytoplankton species, is a fairly good approximation of natural-water composition (even with anomalous natural conditions such as a phytoplankton bloom), as there is always a strong background contribution to the PSD (Twardowski et al., 2001). Besides, it is the only distribution that can be used in the Twardowski model, and therefore, used here. The complex refractive index of Fig. 2b was synthetically generated using imaginary values similar to those presented in Bernard et al. (2009) for phytoplankton species (derived from sample algal assemblages and considering homogeneous spheres). The

BGD
12, 18723–18768, 2015

dependence of the real on the imaginary part of the refractive index can be found in the Kramers–Kronig relations (Bernard et al., 2001, 2009; Bricaud and Morel, 1986; van de Hulst, 1957), which allow the spectral variations in the real refractive index to be calculated as a Hilbert transform of the imaginary refractive index. The central part of the real refractive index was selected as $1 + \epsilon = 1.05$ (for phytoplankton it typically ranges from 1.02 to 1.15, relative to water, as stated in Morel, 1973; Carder et al., 1974; Aas, 1996; Bernard et al., 2001). The effects due to normal dispersion, as described in Aas (1996), have not been considered. As can be seen, the imaginary part presents three peak values, at 440, 500 and 680 nm (corresponding to the chlorophyll absorption wavelengths), and, as expected, a similar shape is propagated to the absorption coefficient spectra, $a(\lambda)$, of Fig. 3a. The volume scattering function at each wavelength is shown in Fig. 3b. As expected (since particles are relatively large regarding to wavelength), the scattering is mainly focused in the forward direction (between 0 and 10°) and smoothly decreases in the backward direction.

4.1.1 The Twardowski model

Equation (15) was applied on this example obtaining the results shown in Fig. 4a. To this end, $\gamma = 0$ since the slop parameter of the PSD $\xi = 3$, and the backscatter fraction was computed with Eq. (9) using the volume scattering phase function values given by the modified BHMIE code. As can be seen, this model obtains a curve shape similar to the absolute value of the original complex refractive index, but with a slight negative offset, presenting an averaged relative error of 42 % (obtained using $|m| - 1$). It must be noted that the Twardowski model was designed for a bulk oceanic distribution presenting different physical properties than those of isolated species of phytoplankton (e.g. index of refraction, shape, etc.), and therefore, it is used here in a different scenario it was designed to.

BGD
12, 18723–18768, 2015

4.1.2 The Stramski model

The results obtained with this model are shown in Fig. 4b. As can be seen, this model overestimates both real and imaginary parts on all the analysed spectra, showing an averaged relative error of 0.4 % for the real part and a 15 % for the imaginary part. It should be remembered that the imaginary part of the refractive index, k_h, is calculated with the ADA, known to give errors of ~ 10 % in comparison to Lorenz–Mie theory (Bernard et al., 2009), and some discrepancies can therefore be expected between ADA and Aden–Kerker derived values.

4.1.3 Genetic algorithm

In order to implement the genetic algorithm described in Sect. 3.4, the tools provided by the DEAP and SCOOP frameworks to develop evolutionary algorithms and parallel task distribution respectively, were used (Fortin et al., 2012). The fitness function was implemented using the fast subroutines of BHMIE to compute the absorption and scattering properties of homogeneous spheres. The coefficients *a* and *b* of Fig. 3a were used as inputs of the genetic algorithm model to estimate the initial complex refractive index and bounding conditions were applied to facilitate the convergence (typical values for the real part of the phytoplankton refractive indices fall within 1.02 and 1.15 relative to water, and the bulk value of the imaginary part is always below 0.02). The genetic algorithm was configured with a vector of 2000 solutions over 10 generations and 50 and 20 % of probability of crossover and mutation respectively, obtaining the estimated values shown in Fig. 5a. The good agreement between the initial complex-refractive-index values and the estimated ones (an averaged relative error of 0.004 % for the real part and 0.24 % for the imaginary part is obtained, presenting thus the best results in this first example) shows that it is possible to perform accurate estimations with a genetic algorithm.

One disadvantage of the genetic algorithms is that they are relatively slow and require more computation time than other optimization algorithms, since they need to

BGD
12, 18723–18768, 2015

execute the fitness function many more times. For comparison purposes, other optimization algorithms were applied to determine if there is the possibility to obtain accurate results with an important reduction of the computation time. Figure 5b shows the results obtained with the much faster Broyden–Fletcher–Goldfarb–Shanno (BFGS) algorithm (BFGS is an iterative method for solving unconstrained nonlinear optimization problems, Zhu et al., 1997), executed using the same bounding conditions as in the genetic algorithm case. In this case, only 224 s (less than 4 min) were needed in front of the 97 min used by the genetic algorithm, both in a PC with an Intel Core i7 processor at 3.2 GHz, a 16 GB RAM and running a Windows 8.1. However, although the results are quite satisfactory in general, some of the wavelengths present a significant error in the real part (mainly, between 550 and 600 nm, and above 680 nm). The averaged relative error is 0.073 % for the real part and 0.72 % for the imaginary part. Other optimization algorithms, such as the conjugated gradient algorithm (Nocedal and Wright, 1999), were also tested. The results, not shown here for space limitations, presented a worse accuracy than the BFGS, showing that the genetic algorithm is probably the optimal method to solve this problem in terms of accuracy (but not in terms of time).

4.2 Spherical-shape coated particles

In order to use the IOPs of a two-layered spherical particle that emulates actual phytoplankton properties, its complex refractive index was generated using the description presented in Bernard et al. (2009). The imaginary refractive index of the inner cytoplasm was obtained using Eq. (20) and its real one using the Hilbert transform and Eq. (17) with $1 + \epsilon = 1.02$. The imaginary refractive index of the outer chloroplast was obtained using Eq. (21), with Vv = 30 % (since it is a value between that assumed by Bernard et al., 2009, and previous works), and its real one using the Hilbert transform and Eq. (17) with $1 + \epsilon = 1.1$. Figure 6a and b show the results for the real and imaginary parts respectively obtained with the BART code, based on the Aden–Kerker theory to calculate light-scattering properties for coated spherical particles, from A. Quirantes (Quirantes, 2005). Instead of using the PSD of Fig. 2a for this example,

BGD
12, 18723–18768, 2015

the PSD of an isolated culture was simulated with a concentration of 40 particles mm^{-3} (R_{min} = 0.7 µm, R_{max} = 12.1 µm). It must be noted that the PSD denotes the external radius (the inner one can be extracted using the Vv value). In this case, the function does not agree with a perfect power-law distribution since there is a minimum size beneath which there are no cells. Thus, the PSD of Fig. 7 (using 31 points) better represents the case of a monoculture PSD. Using this PSD with the previous refractive indices, the absorption, scattering and extinction coefficients of Fig. 8a, and the volume scattering function of Fig. 8b were obtained.

Below, the IOPs presented above are used to estimate their complex refractive indices. First, this is done using the genetic algorithm in order to see if a basic shape such as a homogeneous sphere is useful when modelling more complex particles. If coated particle models better characterize the optical properties of general phytoplankton species, as stated in Bernard et al. (2009), this can be used to estimate the error committed when using spheres. Then, the inner and the outer complex refractive indices of the original particle are retrieved using the Bernard model for coated particles. Finally, a combination of the genetic algorithm and the Bernard model is applied to improve the previous results.

4.2.1 The genetic algorithm

The genetic algorithm model to retrieve the refractive index of spherical-shape homogeneous particles was applied in order to measure the error committed in such approximation. The same configuration as in the previous example was used (an initial vector of 2000 solutions over 10 generations and 50 and 20 % of probabilities for crossovers and mutations respectively). The estimated complex refractive index is shown in Fig. 9a. Both real and imaginary parts present values between the inner and the outer real and imaginary parts of Fig. 6a and b respectively. The volume scattering function generated by the homogeneous particles, as seen in Fig. 9b, shows that this model presents similar values in the forward scattering but completely underestimates

BGD
12, 18723–18768, 2015

the backscattering, presenting values far below those of Fig. 8b. This example demonstrates that the common characterization using homogeneous spheres is not a suitable methodology when dealing with complex particles. Even though it is not a surprising result (this is well known and has been discussed for years, by Bohren and Huffman, 1998, in the atmospheric literature, and by Stramski et al., 2004; Clavano et al., 2007; Dall'Olmo et al., 2009, and Bernard et al., 2009), in the oceanic literature), a comparison between the two volume scattering functions manifests that the backscattering can achieve errors up to one order of magnitude.

4.2.2 The Bernard model

The Bernard model of Sect. 3.3 was used to estimate the complex refractive index of the two-layered particle. Figure 10a shows the initial and estimated real part of the inner and outer layers and Fig. 10b shows the initial and estimated imaginary parts. As expected, the inner refractive index is well estimated (since the same equation is used for both generation and retrieval), but the outer refractive index does not present an accurate agreement. In particular, the imaginary part is meaningfully underestimated, with an averaged relative error of 51 %. On the other hand, the simulation of the estimated refractive indices in coated spheres produce a volume scattering function which is in a better agreement with that of Fig. 8b than the volume scattering function produced by the homogeneous spherical particle (the volume scattering function figure has not been added in this case since errors are not appreciated; a deeper analysis is done in Sect. 5).

4.2.3 The Bernard model combined with genetic algorithm

In order to improve the results presented by the Bernard model in the previous subsection, the genetic algorithm, which showed a suitable performance when applied to homogeneous spherical particles, could be coupled to the BART code (instead the BH-MIE code) to try to estimate the two complex refractive indices. However, results would

BGD
12, 18723–18768, 2015

hardly be accurate since the solution has a higher dimension (the two refractive indices with real and imaginary parts each, that is, four dimensions) than the information data (the attenuation and scattering coefficients, that is, two dimensions). However, there is the possibility to combine the genetic algorithm with the Bernard model to increase the convergence probability. In this case, the inner refractive index is firstly estimated using the Bernard model, as it was done before, and the outer refractive index is obtained secondly with the genetic algorithm (coupled to the BART code). In this case, the genetic algorithm only has to find a solution with two dimensions (the real and imaginary parts of the outer refractive index), more affordable than the whole set of refractive indices.

This method was applied on the coated particle example (using he coefficients of Fig. 8a as input data and configured using an initial vector of 2000 solutions, 10 generations, 50 % of probability for crossovers and 20 % for mutations), obtaining the initial and estimated real part of the inner and outer layers shown in Fig. 11a and the initial and estimated imaginary parts shown in Fig. 11b. As it can be seen, accurate results were obtained, meaningfully improving the refractive index estimation for the outer sphere. In this particular case, an average relative error of 0.01 % was obtained for the real part and a 0.14 % for the imaginary part.

4.3 Cylindrical-shape particles

As a final example, a cylindrical shape particle has been chosen. As commented above, phytoplankton species usually present complex shapes, far from perfect homogeneous or coated spheres (as it is the case of the diatom *Thalassiosira pseudonana*). In order to find which is the most accurate model for the characterization of such complex shapes, an example considering 100 prolate cylinders mm^{-3} with a diameter-to-length ratio equivalent to 0.8, the PSD of Fig. 12 (showing the radius of an equivalent volume sphere with a slop parameter $\xi = 3$, effective radius $r_{eff} = 3.2\,\mu m$ and effective variance $v_{eff} = 0.005$ resulting in $R_{min} = 0.8\,\mu m$ to $R_{max} = 3.6\,\mu m$), and the initial refractive index of Fig. 2b was simulated using the **T** Matrix characterization (Mischenko et al., 1996;

BGD
12, 18723–18768, 2015

Mischenko and Travis, 1998). To this end, the code from M. Mischenko (Mischenko and Travis, 1998) for **T** Matrix computations on randomly oriented, rotationally symmetric scatterers (cylinders, spheroids and Chebyshev particles) was used. The PSD presents a small effective variance for convergence limitations of the code. The initial $a(\lambda)$, $b(\lambda)$ and $c(\lambda)$ coefficients are shown in Fig. 13a, and the volume scattering function at each wavelength is shown in Fig. 13b.

4.3.1 The Bernard model combined with genetic algorithm

Even though this IOP is not an exact copy of an actual phytoplankton IOP (for the reasons commented before), the coated sphere model is used here to model the cylindrical shape to analyse their differences. Figure 14a shows the initial and estimated real part of the inner and outer layers and Fig. 14b shows the initial and estimated imaginary parts. The volume scattering function is shown in Fig. 15. The committed error in this last figure is noticeable even to the naked eye, especially at higher wavelengths, achieving an averaged relative error of 77 %. It should be noted that these differences may decrease when using real phytoplankton, since backscattering of heterogeneous particles is different from that of homogeneous particles.

4.3.2 The genetic algorithm

One possible action could be exerted using the genetic algorithm combined with the **T** Matrix code in order to consider cylindrical shapes when estimating the inner complex refractive index. However, one simulation of cylindrical shape particles with such dimensions, using the Mischenko code, needs about 67 min in a computer with an i7 at 3.20 GHz and running Windows 8.1. This prevents the use of the genetic algorithm in such circumstances, since it needs to execute this simulation several hundreds of times at each wavelength in order to accurately estimate the complex refractive index. That means that several months would be required to estimate the whole refractive index spectra, even using distributed processing. To avoid that, some kind of approximations

BGD
12, 18723–18768, 2015

must be considered. In order to perform fast estimations, equal-volume homogeneous particles with spherical shape are considered instead of the cylinders. This allows using the Lorenz–Mie theory instead the **T** Matrix approach, dramatically improving the simulation time. Then, the estimated refractive index using homogeneous spheres is finally applied on homogeneous cylinders to obtain their IOP, since the volume scattering function values are case sensitive to the particle shape. Although the slow **T** Matrix approach is needed for this simulation, it has to be executed only once.

The methodology was applied on this last example using the same PSD of Fig. 12. The estimated complex refractive index is shown in Fig. 16a. The averaged relative error of the real part is 7.75 and 2.61 % for the imaginary part. The major differences are obtained at the lowest wavelengths, which is also noticeable in the volume scattering function, as seen in Fig. 16b, with some artefacts in those wavelengths where abrupt changes of the real part of the refractive index occur (330 and 350 nm). However, the averaged relative error committed decreases from 77 % in the previous method to 16 %. If homogeneous spheres are used instead of cylinders to obtain the IOP, the averaged relative error increases to 22 %, which demonstrates that choosing a suitable shape improves the results.

5 Discussion

Table 1 shows the averaged relative errors associated with each method when estimating the real and imaginary parts of the refractive indices and the one committed by the respective volume scattering functions in the three examples of the previous section. In the real part case, the error was obtained using $n - 1$ instead of n.

In the homogeneous sphere example, only the errors committed by the Stramski model and the Genetic Algorithm are shown, since the Twardowski model computes the bulk refractive index, and real and imaginary parts cannot be separated. Thus, neither can its volume scattering function be obtained. If compared with the absolute value of the original complex refractive index, an averaged relative error of 42 % is obtained.

BGD
12, 18723–18768, 2015

It can also be seen in the table that, although the errors of the Stramski model are considerably higher than the ones of the Genetic Algorithm, specially in the imaginary part estimation, similar estimations of the volume scattering function are recovered in both cases. This implies that there is no need of an accurate refractive index estimation in this particular example to obtain a suitable characterization of the scattering properties. However, the Genetic Algorithm performs with an extreme accuracy for the refractive-index retrieval.

In the coated sphere example, the Genetic Algorithm approximates the coated particle to a homogeneous one with a single complex refractive index. Therefore, errors for the inner and outer refractive indices cannot be obtained. Besides, this method presents an important disagreement when computing the volume scattering function. This result shows that, in case the optical behaviour of coated spheres were closer to that of actual phytoplankton particles, as stated in (Bernard et al., 2009), homogeneous spheres would not be a suitable choice to accurately reproduce their optical behaviour. The Bernard model is a fast technique to estimate the inner and outer refractive indices, but mainly fails in estimating the imaginary part of the refractive index (with an error up to 51 %). This leads to a significant error committed by the computed volume scattering function. However, if the Bernard model is combined with the Genetic Algorithm (the Bernard model is used to estimate the inner refractive index, and the Genetic Algorithm to retrieve the external one), accurate values are obtained for the complex refractive indices and for the volume scattering function.

Finally, in the homogeneous cylinder case, it can be seen that the optical properties of this kind of particles are not accurately reproduced using a coated sphere which refractive indices are obtained with the combination of the Bernard model and the Genetic Algorithm. From the previous results, it could be expected that the optimal retrieval method would be the Genetic Algorithm using cylindrical shapes to obtain an accurate estimation. However, this involves using the slow **T** Matrix code of Mischenko, which would require several months to converge (as the particle becomes more aspherical, the convergence time increases considerably). In order to make the retrieval faster,

BGD
12, 18723–18768, 2015

homogeneous spheres with equal volume are used instead of cylinders. The retrieved refractive index is then used to obtain the IOPs using cylinders this time. Using this method, the volume scattering function shows an averaged relative error of 16 %, improving the result obtained using spheres (22 %). Therefore, this result confirms that selecting a suitable shape is important for an improvement of the modelling (at least in this ideal case).

To conclude, the results presented in Table 1 do not determine which is the best method to estimate phytoplankton optical properties but which one is more accurate when retrieving the refractive index of some ideal particles (such as homogeneous and coated spheres or cylinders). However, synthetic particles serve as a first approximation of actual phytoplankton and are useful to extract some preliminary conclusions. Most of the methods shown in the paper are used for the retrieval of the refractive indices of isolated particles or bulk oceanic distributions, and a comparison of their performance can only be done using well-known models. As it has been shown on each example, the Genetic Algorithm is a versatile technique that alone or combined with other methods improve the accuracy of the estimations. However, it is not a fast technique, and several minutes are required for each estimation (when using spherical shapes; slower with aspherical particles) in front of the few seconds required by the other methods, being the Twardowski model the faster of them.

Further work must be done in order to study their performance when using the optical properties of actual phytoplankton species and bulk oceanic measurements. New shapes may be required to improve the results, as for instance coated cylinders to model algae with a cylindrical shape (as stated by Bernard et al., 2009, in the spherical case, coated particles generate backscattering functions closer to those produced by actual phytoplankton particles) or other outlines more similar to the actual shape of the particle (the **T** Matrix approach allows the computation of particle shapes performing axial symmetry). There is, however, one important disadvantage shared by all the methods described in this paper, and it is their strong dependence on the accuracy of the measurements. Attenuation and scattering coefficients are needed as inputs for all

BGD
12, 18723–18768, 2015

of the retrieval methods, and if they are not accurate, the retrieved refractive indices will not be as well. As stated by Ramírez-Pérez et al. (2015), the acceptance angle of the optical instruments affect severely on the amplitude of the measurements. By comparing the extinction coefficient of two different instruments with different acceptance angles, different magnitude values were obtained, showing an averaged ratio of 0.67. This is a key issue that must be considered and dealt in order to improve the faithfulness of the whole methodology. Otherwise, the accuracy of the retrieval methods, as studied here, is useless.

6 Conclusions

A performance analysis was carried out in order to examine the accuracy of different inverse methods that use the optical properties of small scatterers and their particle size distribution to retrieve their refractive indices. To this end, three different synthetic examples were contemplated, each one with a different shape and distribution. The selected shapes were homogeneous spheres, coated spheres and homogeneous cylinders. Results evidenced that those methods using a genetic algorithm to optimize the inversion were the most accurate ones, but also the slowest. In particular, an excellent agreement between estimated and actual refractive indices and volume scattering functions was obtained for the homogeneous and coated sphere cases, and a fair agreement for the homogeneous cylinder. These results suggest that better characterizations could be obtained for the actual phytoplankton optical properties. Therefore, next step is a further analysis of the performance of these methods when applied on measurements of isolated cultures of phytoplankton.

Acknowledgements. This work was supported by the Spanish National Research Council (CSIC) under the EU Citclops Project (FP7-ENV-308469).

BGD
12, 18723–18768, 2015

References

Aas, E.: Refractive index of phytoplankton derived from its metabolite composition, J. Plankton Res., 18, 2223–2249, 1996. 18725, 18737

Andrady, A.: Microplastics in the marine environment, Mar. Pollut. Bull., 62, 1596–1605, 2011. 18724

Bernard, S., Probyn, T., and Barlow, R.: Measured and modelled optical properties of particulate matter in the southern Benguela, S. Afr. J. Sci., 97, 410–420, 2001. 18725, 18732, 18737

Dutreuil, S., Bopp, L., and Tagliabue, A.: Impact of enhanced vertical mixing on marine biogeochemistry: lessons for geo-engineering and natural variability, Biogeosciences Discuss., 6, 1–26, doi:10.5194/bgd-6-1-2009, 2009. 18725, 18732, 18733, 18735, 18736, 18737, 18738, 18739, 18740, 18741, 18745, 18746

Bhandarkar, S., Zhang, Y., and Potter, W.: An edge detection technique using genetic algorithm-based optimization, Pattern Recogn., 27, 1159–1180, 1994. 18735

Bohren, C. and Huffman, D. (Eds.): Absorption and Scattering of Light by Small Particles, Wiley, New York, Oxford, 1998. 18727, 18729, 18736, 18741

Boss, E., Pegau, W., Gardner, W., Zaneveld, J., Barnard, A., Twardowski, M., Chang, G., and Dickey, T.: Spectral particulate attenuation and particle size distribution in the bottom boundary layer of a continental shelf, J. Geophys. Res., 106, 9509–9516, 2001a. 18731

Boss, E., Twardowski, M., and Herring, S.: Shape of the particulate beam attenuation spectrum and its inversion to obtain the shape of the particulate size distribution, Appl. Optics, 40, 4885–4893, 2001b. 18731

Boss, E., Pegau, W., Lee, M., Twardowski, M., Shybanov, E., Korotaev, G., and Baratange, F.: Particulate backscattering ratio at LEO 15 and its use to study particles composition and distribution, J. Geophys. Res., 109, C01014, doi:10.1029/2002JC001514, 2004. 18731

Bricaud, A. and Morel, A.: Light attenuation and scattering by phytoplanktonic cells: a theoretical modeling, Appl. Optics, 25, 571–580, 1986. 18725, 18729, 18731, 18737

Bricaud, A., Zaneveld, J., and Kitchen, J.: Backscattering efficiency of coccol-25 ithophorids: use of a three-layered sphere model, in: Ocean Optics XI Proc SPIE, San Diego, CA, 19 July, 27–33, 1992. 18733

Carder, K., Betzer, P., and Eggimann, D. W. (Eds.): Physical, chemical, and optical measures of suspended particle concentrations: their intercomparison and application to the west African shelf, in: Suspended Solids in Water, Springer US, Oxford, 173–193, 1974. 18737

BGD
12, 18723–18768, 2015

Clavano, W., Boss, E., and Karp-Boss, L.: Inherent optical properties of non-spherical marine-like particles – from theory to observation, Oceanogr. Mar. Biol., 45, 1–38, 2007. 18725, 18741

Cole, M., Lindeque, P., Halsband, C., and Galloway, T.: Microplastics as contaminants in the marine environment: a review, Mar. Pollut. Bull., 62, 2588–2597, 2011. 18724

Dall'Olmo, G., Westberry, T. K., Behrenfeld, M. J., Boss, E., and Slade, W. H.: Significant contribution of large particles to optical backscattering in the open ocean, Biogeosciences, 6, 947–967, doi:10.5194/bg-6-947-2009, 2009. 18741

Fortin, F., Rainville, F. D., Gardner, M., Parizeau, M., and Gagné, C.: DEAP: evolutionary algorithms made easy, Machine Learning Research, 13, 2171–2175, 2012. 18738

Greenhalgh, D. and Marshall, S.: Convergence criteria for genetic algorithms, J. Computing, 30, 269–282, 2000. 18734

Hale, G. and Querry, M.: Optical constants of water in the 200 nm to 200 µm wavelength region, Appl. Optics, 12, 555–563, 1973. 18730

Latimer, P.: Light scattering by a homogeneous sphere with radial projections, Appl. Optics, 23, 442–447, 1984. 18733

Mera, N., Elliott, L., and Ingham, D. B.: A multi-population genetic algorithm approach for solving ill-posed problems, Comput. Mech., 33, 254–262, 2004. 18735

Meyer, R.: Light-scattering from biological cells – dependence of backscatter radiation on membrane thickness and refractive index, Appl. Optics, 18, 585–588, 1979. 18725, 18732

Mischenko, M. and Travis, L.: Capabilities and limitations of a current Fortran implementation of the *T* Matrix method for randomly oriented, rotationally symmetric scatterers, J. Quant. Spectrosc. Ra., 60, 309–324, 1998. 18729, 18743

Mischenko, M., Travis, L., and Mackowski, D.: *T* Matrix computations of light scattering by non-spherical particles: a review, J. Quant. Spectrosc. Ra., 55, 535–575, 1996. 18727, 18729, 18742

Morel, A.: Diffusion de la lumière par les eaux de mer; résultats expérimentaux et approche théorique, in: Optics of the Sea, AGARD Lecture Ser., vol. 61, Advisory Group for Aeronautical Research and Development, NATO, Brussels, 3.1.1.–3.1.76, 1973. 18737

Mugnai, A. and Wiscombe, W.: Scattering from nonspherical Chebyshev particles. I: Cross sections, single-scattering albedo, asymmetry factor, and backscattered fraction, Appl. Optics, 25, 1235–1244, 1986. 18729

Nocedal, J. and Wright, S. (Eds.): Numerical Optimization, Springer, New York, 1999. 18739

BGD

12, 18723–18768, 2015

Quirantes, A.: A *T* Matrix method and computer code for randomly oriented, axially symmetric coated scatterers, J. Quant. Spectrosc. Ra., 92, 373–381, 2005. 18739

Quirantes, A. and Bernard, S.: Light-scattering methods for modelling algal particles as a collection of coated and/or nonspherical scatterers, J. Quant. Spectrosc. Ra., 100, 315–324, 2006. 18725

Ramírez-Pérez, M., Röttgers, R., Torrecilla, E., and Piera, J.: Cost-effective hyperspectral transmissometers for oceanographic applications: performance analysis, Sensors, 15, 20967–20989, 2015. 18747

Sánchez, A., Zafra, E., and Piera, J.: Hyperspectral characterization of marine particles based on Mie–Lorentz and *T* Matrix codes and a genetic algorithm, in: IEEE Workshop on Hyperspectral Image and Signal Processing: Evolution in Remote Sensing (WHISPERS), Lausanne, Switzerland, 24–27 June 2014. 18725, 18733

Stramski, D., Morel, A., and Bricaud, A.: Modeling the light attenuation and scattering by spherical phytoplanktonic cells: a retrieval of the bulk refractive index, Appl. Optics, 27, 3954–3956, 1988. 18725, 18731

Stramski, D., Bricaud, A., and Morel, A.: Modeling the inherent optical properties of the ocean based on the detailed composition of the planktonic community, Appl. Optics, 40, 2929–2945, 2001. 18725, 18736

Stramski, D., Boss, E., Bogucki, D., and Voss, K.: The role of seawater constituents in light backscattering in the ocean, Prog. Oceanogr., 61, 27–56, 2004. 18741

Twardowski, M., Boss, E., Macdonald, J., Pegau, W., Barnard, A., and Zaneveld, J.: A model for estimating bulk refractive index from the optical backscattering ratio and the implications for understanding particle composition in case I and case II waters, Geophys. Res. Oceans, 106, 14129–14142, 2001. 18725, 18729, 18730, 18731, 18736, 18756

van de Hulst, H. (ed.): Ligh Scattering by Small Particles, Wiley, New York, Oxford, 1957. 18730, 18731, 18732, 18737

Volz, F.: Die Optik und Meteorologie der Atmosphärishen Trübung, Ber. Dtsch. Wetterdienstes, 13, 1–47, 1954. 18730

Wiscombe, W. and Grams, G.: The backscatered fraction in two-stream approximations, J. Atmos. Sci., 33, 2440–2451, 1976. 18729

Zaneveld, J. and Kitchen, J.: The variation in the inherent optical properties of phytoplankton near an absorption peak as determined by various models of cell structure, Geophys. Res., 100, 13309–13320, 1995. 18733

BGD
12, 18723–18768, 2015

Zhu, C., Byrd, R., and Nocedal, J.: L-BFGS-B: algorithm 778: L-BFGS-B, FORTRAN routines for large scale bound constrained optimization, ACM T. Math. Software, 23, 550–560, 1997. 18739

BGD
12, 18723–18768, 2015

Table 1. Averaged relative errors committed in each method.

Shapes	Model	n relative error	k relative error	VSF relative error
Homogeneous sphere	Twardowski model	–[a]	–	–
	Stramski model	8.2 %	15 %	0.17 %
	Genetic Algorithm	0.08 %	0.24 %	0.17 %
Coated sphere	Genetic Algorithm	–	–	78 %
	Bernard model	1.4 %	51 %	52 %
	Bernard model and GA	0.1 %	0.14 %	0.2 %
Homogeneous cylinder	Bernard model and GA	–	–	77 %
	Genetic Algorithm[b]	7.75 %	2.61 %	16 %[c]

[a] The bulk refractive index presents an error of 42 % if it is compared with $|m|$.
[b] The refractive index is estimated using spheres but the IOP is obtained using that refractive index in cylinders.
[c] If the cylindrical shape is not used, the error rises up to 22 %.

BGD
12, 18723–18768, 2015

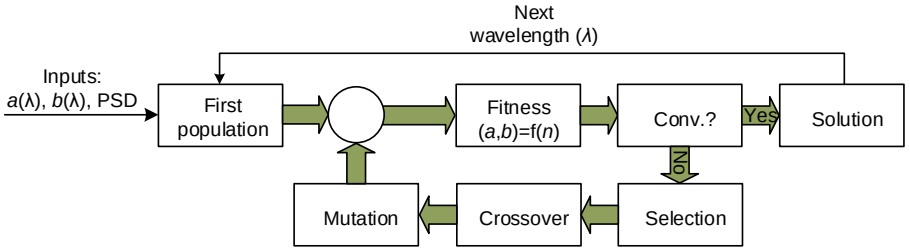

Figure 1. Flow chart of the genetic algorithm.

BGD
12, 18723–18768, 2015

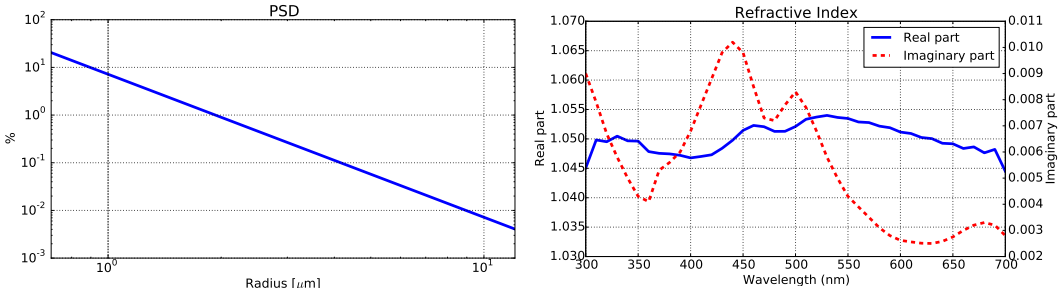

Figure 2. (a) PSD of the example with spherical-shape homogeneous particles. **(b)** Synthetic complex refractive-index signature of the example with spherical-shape homogeneous particles.

BGD
12, 18723–18768, 2015

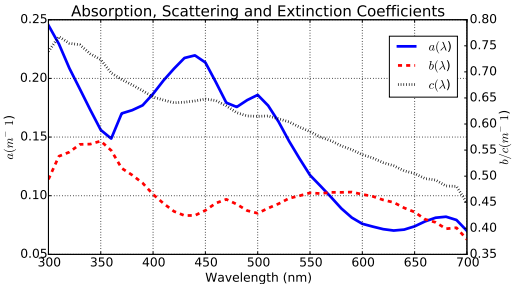

(a)

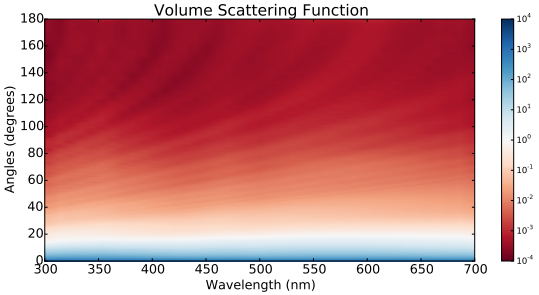

(b)

Figure 3. (a) Absorption (a), scattering (b) and extinction (c) coefficients of the example with spherical-shape homogeneous particles, and **(b)** the volume scattering function.

BGD
12, 18723–18768, 2015

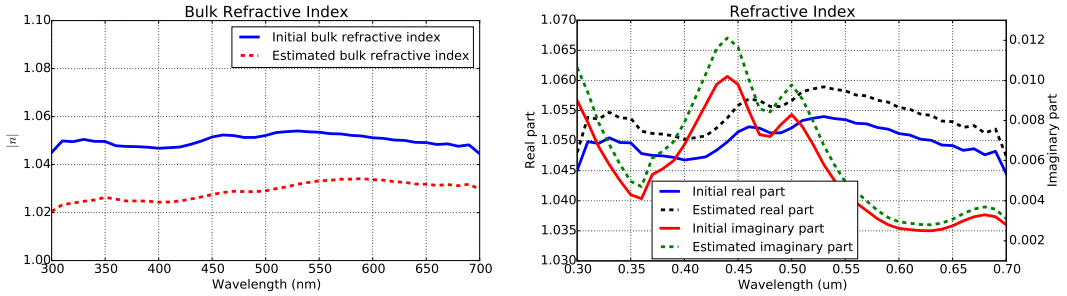

Figure 4. (a) Estimated bulk refractive index obtained from the model of Twardowski et al. (2001) compared with the absolute value of the initial complex refractive index. **(b)** Initial and estimated refractive indices using the Bernard model.

BGD
12, 18723–18768, 2015

Methods comparison to retrieve the refractive index of small scatterers

A.-M. Sánchez and J. Piera

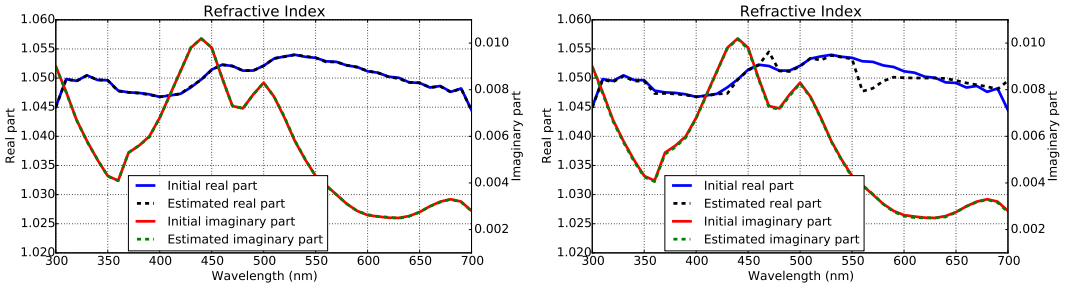

Figure 5. (a) Initial and estimated refractive indices using the genetic algorithm presented in this paper. **(b)** Initial and estimated refractive indices using the BFGS algorithm.

BGD
12, 18723–18768, 2015

Methods comparison to retrieve the refractive index of small scatterers

A.-M. Sánchez and J. Piera

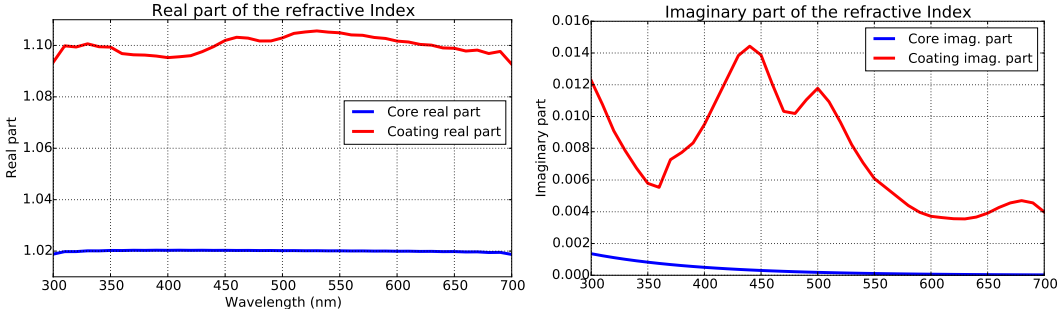

Figure 6. (a) Synthetic real refractive-index signatures for the inner and outer layers. **(b)** Synthetic imaginary refractive-index signatures for the inner and outer layers.

BGD
12, 18723–18768, 2015

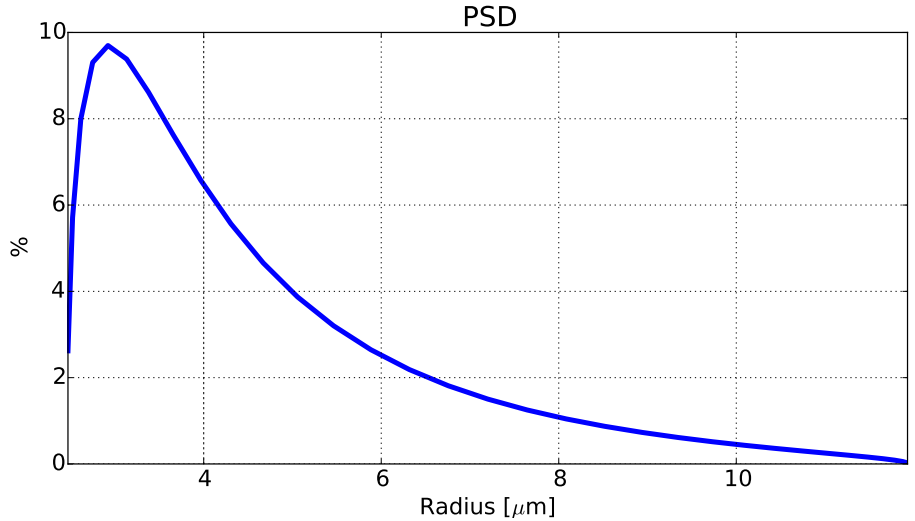

Figure 7. PSD that simulates a an isolated culture.

BGD
12, 18723–18768, 2015

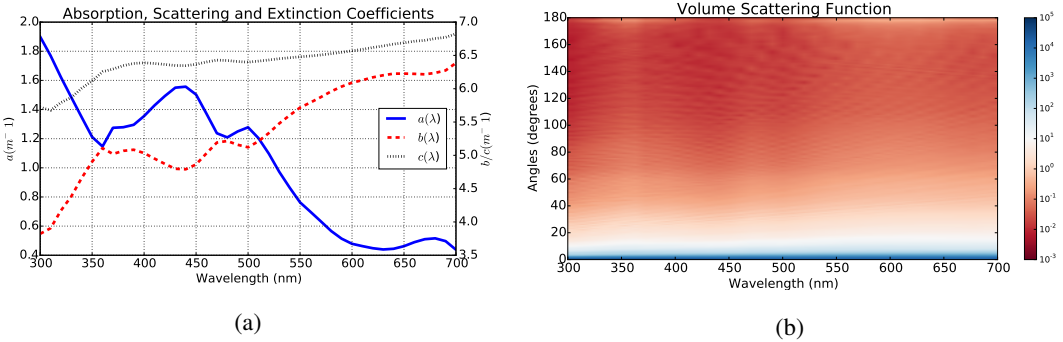

(a) (b)

Figure 8. (a) Absorption (a), scattering (b) and extinction (c) coefficients of the coated-particle example, and **(b)** the volume scattering function.

BGD
12, 18723–18768, 2015

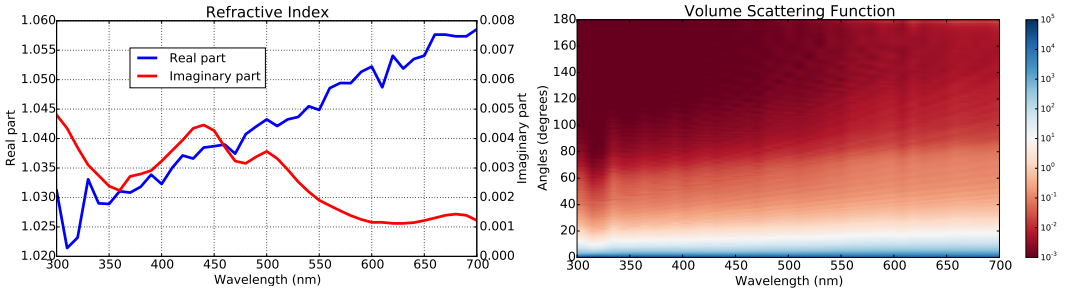

(a) (b)

Figure 9. (a) Complex refractive-index signature estimated using the genetic algorithm model in the second example. **(b)** Volume scattering function using the estimated refractive index in the second example.

BGD
12, 18723–18768, 2015

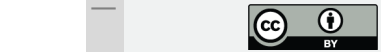

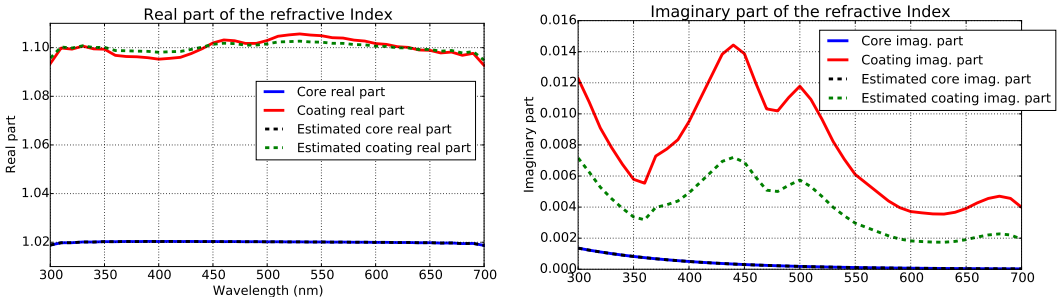

(a) (b)

Figure 10. (a) Initial and estimated real part of the refractive indices for the inner and outer layers using the Bernard model. **(b)** Initial and estimated imaginary part of the refractive indices for the inner and outer layers using the Bernard model.

BGD
12, 18723–18768, 2015

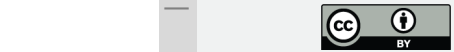

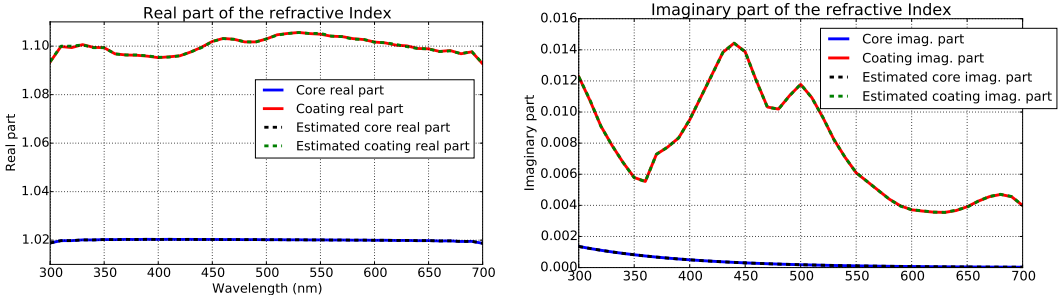

(a) (b)

Figure 11. (a) Initial and estimated real part of the refractive indices for the inner and outer layers using the Bernard model combined with the genetic algorithm. **(b)** Initial and estimated imaginary part of the refractive indices for the inner and outer layers using the Bernard model combined with the genetic algorithm.

BGD
12, 18723–18768, 2015

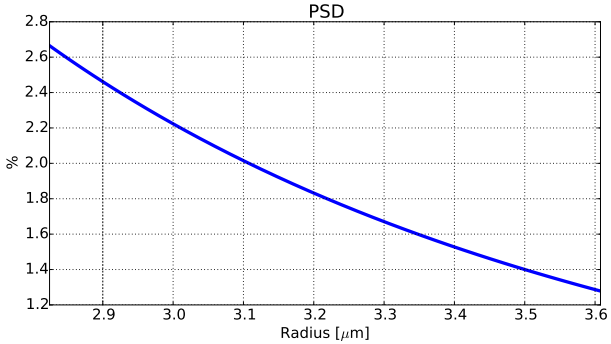

Figure 12. PSD of the cylindrical-shape example.

BGD
12, 18723–18768, 2015

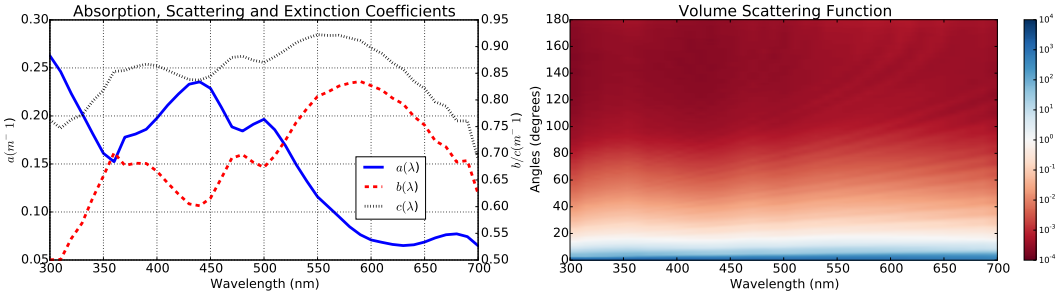

(a) (b)

Figure 13. (a) Absorption (*a*), scattering (*b*) and extinction (*c*) coefficients of the cylindrical-shape example. **(b)** Volume scattering function of the cylindrical-shape example.

BGD
12, 18723–18768, 2015

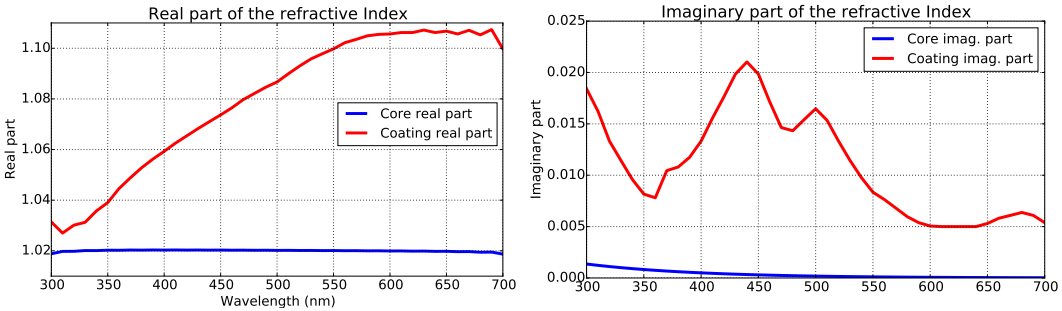

(a) (b)

Figure 14. (a) Inner and outer real part of the refractive indices using the Bernard Model combined with Genetic Algorithm in the cylindrical example. **(b)** Inner and outer imaginary part of the refractive indices using the Bernard Model combined with Genetic Algorithm in the cylindrical example.

BGD
12, 18723–18768, 2015

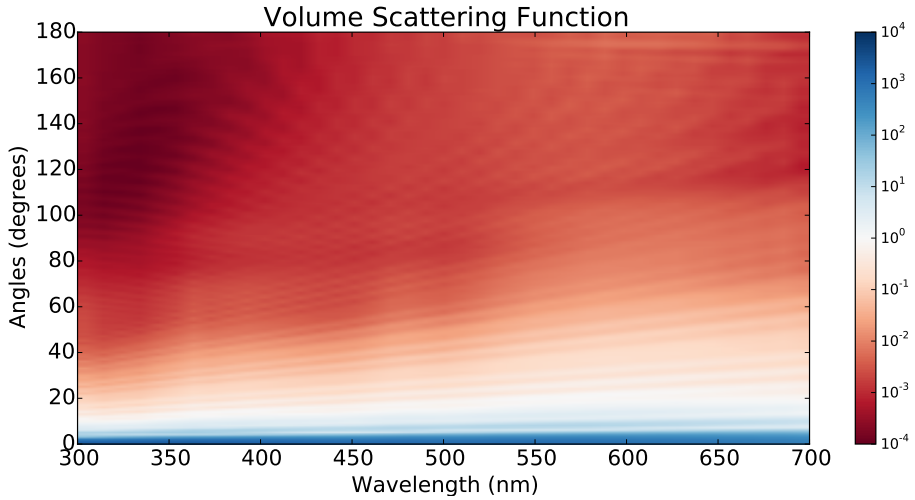

Figure 15. Volume scattering function obtained using the Bernard Model combined with Genetic Algorithm in the cylindrical example.

BGD
12, 18723–18768, 2015

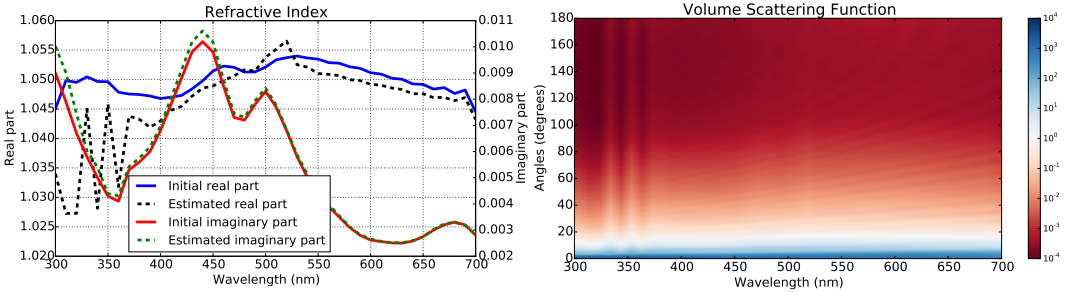

(a) (b)

Figure 16. (a) Initial and estimated refractive indices using the genetic algorithm for spherical-shape homogeneous particles, and **(b)** the volume scattering function.

BGD
12, 18723–18768, 2015